Dalton Transactions

ROYAL SOCIETY OF CHEMISTRY

PAPER

View Article Online
View Journal | View Issue

Cite this: *Dalton Trans.*, 2025, **54**, 10085

Sulfate-modified MOF-808 as a superacid catalyst: a performance evaluation of Zr(IV) and Hf(IV) analogues in acetalization reactions†

Vanesa Roa,[a] Sebastian Cea,[a] César Pazo,[e] Jaime Llanos,[b] Douglas Olivares,[c] Néstor Escalona,[e] Ángel Leiva,[f] Yoan Hidalgo-Rosa,[g] Ximena Zarate,[d] Ana Belen Dongil[h] and Eduardo Schott*[a]

Received 13th March 2025,
Accepted 19th May 2025

DOI: 10.1039/d5dt00608b

rsc.li/dalton

In this study, we report the synthesis and characterization of MOF-808-SO_4-M (M = Zr(IV), Hf(IV)), derived from MOF-808-M precursors. The introduction of sulfate groups enhances the Brønsted acidity of these materials, significantly improving their catalytic performance in the benzaldehyde acetalization reaction. The materials were characterized using powder X-ray diffraction (PXRD), Fourier-transform infrared spectroscopy (FT-IR), nitrogen adsorption–desorption analysis, thermogravimetric analysis (TGA), energy-dispersive spectroscopy (EDS), and Hammett indicator tests. Catalytic evaluation revealed that MOF-808-SO_4-Zr exhibited significantly higher conversion compared to its Hf-based analogue, a difference attributed to its greater density of acid sites, as confirmed by temperature-programmed surface reaction (TPSR) analysis. These experimental results were further supported by density functional theory (DFT) calculations, which provided insights into the acidic properties and catalytic behavior of the materials.

Introduction

Lignocellulosic biomass derived from forestry and agricultural waste is the most abundant form of natural biomass worldwide and has garnered significant attention as a sustainable raw material for energy production.[1] This growing interest is driven by the depletion of fossil fuel resources and the environmental impact of large-scale fossil fuel combustion, which contributes to climate change.[2,3] Consequently, the development of renewable energy sources and alternative fuels from biomass derivatives presents a promising and sustainable solution to these challenges.[4]

Biomass is primarily composed of aromatic compounds, making it a valuable source of platform molecules that serve as precursors for producing high-value chemical compounds.[5–7] One such example is aromatic aldehydes, which undergo acetalization to form acetals—key products widely used in the food and pharmaceutical industries.[8,9] This reaction requires a catalyst with acidic sites in its structure.[10] The most commonly used catalysts for acetalization are homogeneous catalysts, such as mineral acids like hydrochloric acid (HCl).[8,10] However, these catalysts generate large amounts of waste and are not easy to separate from the obtained products.[11]

Metal–organic frameworks (MOFs) have emerged as a promising alternative in heterogeneous catalysis.[12] As a subfamily of coordination polymers (CPs), MOFs consist of metal clusters and organic ligands, commonly referred to as linkers, which assemble into highly ordered three-dimensional structures.[13,14] Their exceptional properties, including high porosity, large surface area, and high crystallinity, have expanded their range of applications.[14,15] MOFs have been extensively studied for use in

[a]*Departamento de Química Inorgánica, Facultad de Química y de Farmacia, Centro de Energía UC, Centro de Investigación en Nanotecnología y Materiales Avanzados CIEN-UC, Pontificia Universidad Católica de Chile, Avenida Vicuña Mackenna, 4860 Santiago, Chile. E-mail: maschotte@gmail.com*
[b]*Departamento de Química, Facultad de Ciencias, Universidad Católica del Norte, Avda. Angamos 0610, Antofagasta 1270709, Chile*
[c]*Centro de Desarrollo Energético Antofagasta, Universidad de Antofagasta, Antofagasta, Angamos 601, Antofagasta, 1270300, Chile*
[d]*Instituto de Ciencias Aplicadas, Facultad de Ingeniería, Universidad Autónoma de Chile, Santiago, Chile*
[e]*Departamento de Ingeniería Química y Bioprocesos, Escuela de Ingeniería, Pontificia Universidad Católica de Chile, Avenida Vicuña Mackenna 4860, Macul, Santiago, Chile*
[f]*Departamento de Química-Física, Facultad de Química y Farmacia, Pontificia Universidad Católica de Chile, Avenida Vicuña Mackenna 4860, Macul, Santiago, Chile*
[g]*Centro de Nanotecnología Aplicada, Facultad de Ciencias, Ingeniería y Tecnología, Universidad Mayor, Camino La Pirámide 5750, Huechuraba, Santiago, 8580745, Chile*
[h]*Instituto de Catalisis y Petroleoquimica (ICP), CSIC, C/Marie Curie 2, 28049 Madrid, España*

† Electronic supplementary information (ESI) available. See DOI: https://doi.org/10.1039/d5dt00608b

gas storage,[16] catalysis,[12] drug adsorption,[17] and separation membranes,[18] highlighting their versatility and potential in various industrial and scientific fields.

Due to the presence of different kinds of acid sites, which could be located on the metal centers or the linkers, MOFs hold great potential for the development of novel superacid materials.[19] Their acidity can be assessed using the Hammett function, a measure of acidity beyond the conventional pH scale, specifically designed for non-aqueous systems and extremely strong acids.[20] On this scale, MOFs exhibit a Hammett function (H_0) of ≤ -12.2, indicating their strong acidic nature. Notably, materials such as MOF-808 have demonstrated high stability and enhanced Brønsted acidity when functionalized with sulfonated groups or hydroxyl ligands, further reinforcing their classification as superacids.[19–21]

MOF-808 possesses both Lewis and Brønsted acid sites, offering enhanced structural accessibility due to the number of ligands present in its framework. MOF-808-Zr consists of Zr(IV) metal centers that form Secondary Building Units (SBUs) connected by benzene-1,3,5-tricarboxylic acid (BTC) tritopic bonds, resulting in a connectivity of six at each Zr node. The structure comprises six BTC units, generating two distinct pore sizes: a larger octahedral pore (16 Å) and a smaller tetrahedral pore (1.2 Å), the latter being less accessible to guest molecules.

In 2014, the first reported superacid MOF based on a Zr-based framework, MOF-808, was synthesized. In that report, the superacidity of MOF-808 was demonstrated by introducing sulfuric acid (H_2SO_4), which replaced the formate groups of the SBUs with sulfate ligands, forming MOF-808-SO_4.[21] MOF-808 consists of $Zr_6O_4(OH)_4(CO_2)_6$ clusters coordinated with 1,3,5-benzenetricarboxylate (BTC) linkers.[22] Specifically, the structure comprises six BTC units, generating two distinct pore sizes: a larger octahedral pore (16 Å) and a smaller tetrahedral pore (1.2 Å), the latter being less accessible to guest molecules.[23] The modified material (sulfated structure) was prepared by soaking MOF-808 in aqueous sulfuric acid, facilitating the replacement of non-structural formate groups with sulfate ligands on the metal clusters, thereby enhancing its acidity.[19] In a previous study, we explored MOF-808-M synthesized with Zr(IV), Hf(IV), and Ce(IV).[24] In this report, we focus on the post-synthetic modification of MOF-808-M by varying the metal center (M) between Zr(IV) and Hf(IV). Upon treatment with H_2SO_4, these materials yield MOF-808-SO_4-Zr and MOF-808-SO_4-Hf.[20] The obtained materials were characterized using techniques such as powder X-ray diffraction (PXRD), Fourier transform infrared spectroscopy (FT-IR), N_2 adsorption, thermogravimetric analysis (TGA), potentiometric titration, scanning electron microscopy-energy dispersive spectroscopy (SEM-EDS), and the Hammett indicator test. Furthermore, the influence of the metal center on the superacid MOFs (herein referred to as MOF-808-SO_4-Zr and MOF-808-SO_4-Hf) was systematically evaluated for the first time as catalysts in the acetalization of benzaldehyde with methanol, yielding (dimethoxymethyl)benzene. A significant enhancement in catalytic activity was observed for these sulfated materials compared to their non-sulfated counterparts,[24] highlighting the beneficial impact of sulfate functionalization on their acidity and performance. Additionally, density functional theory (DFT) calculations of a reduced MOF-808-SO_4-M model were performed to support the experimentally observed catalytic behavior.

Methodology

In this work, unless otherwise stated, all chemicals involved are commercially available and were used as received without further purification.

Materials and methods

Zirconium(IV) chloride anhydrous ($ZrCl_4$, 98%, Acros Organics), hafnium(IV) chloride ($ZrCl_4$, 99.9%, Strem Chemicals), benzene-1,3,5-tricarboxylic acid (H_3BTC, 98%, Merck), *N*,*N*-dimethylformamide (DMF, 99%, Merck), formic acid for analysis (HCOOH, 98–100%, Merck), benzaldehyde for synthesis (99%, Merck), sulfuric acid (97%, Merck), chloroform (99.5%, Merck), methanol (99.5%, Merck), naphthalene (99%, Sigma-Aldrich), and acetone (99%, Winkler) were used as obtained. PXRD characterization for product identification was performed on a D2 PHASER Bruker with Mo Kα1 radiation. For the textural determination, MOF-808-SO_4-Zr and MOF-808-SO_4-Hf were activated for 24 hours at 150 °C under vacuum using a VACPREP 061. The determination of the specific area of each adsorbent was done using a Micromeritics 3FLEX apparatus for volumetric nitrogen adsorption–desorption. The Brunauer–Emmett–Teller (BET) method was used to determine the specific areas according to the Rouquerol criteria, and the pore size was determined by the Horvath–Kawazoe (HK) method.[25] The Fourier-transform infrared (FT-IR) spectra were recorded with an attenuated total reflectance (ATR) accessory using IRSpirit equipment, SHIMADZU. Thermogravimetric measurements were performed on a TGA/SDTA851 Mettler-Toledo thermobalance; the sample was heated from 20 °C to 900 °C at a 20 °C min^{-1} slope under a constant nitrogen flow.

Synthesis of MOF-808-SO_4-Zr

The synthesis of precursors was realized using the method reported in previous work; see the ESI† for further details.[24] The synthesis of the sulfate derivative was performed following a previous report by Yaghi *et al.*[20] In summary, activated MOF-808-Zr microcrystalline powder (0.50 g) was immersed in 50 mL of 0.1 M sulfuric acid (5 mmol) for 24 h, with the mixture stirred once every two hours. The solution was then decanted, and the remaining solid material was then solvent exchanged with 50 mL of water for three days (water exchanged three times per day), followed by a quick exchange with 5 × 50 mL of anhydrous acetone and immersion in 50 mL of anhydrous chloroform for three days. During the chloroform immersion, the solvent was exchanged three times per day. The chloroform-exchanged material was activated under dynamic vacuum (30 mTorr) for 24 h at room temperature and 24 h at 150 °C. The obtained material was stored in a glovebox to prevent hydration. The MOF-808-SO_4-Hf material was obtained using the same methodology, with MOF-808-Hf as the precursor.

Hammett indicator test

This test was performed with the method reported in the literature.[20] A set of stock Hammett indicator solutions (0.5 wt%) was prepared in an inert atmosphere glovebox by dissolving Hammett indicators in anhydrous benzene. Hammett indicator stock solution (5 mL) was added to 20 mg of each activated MOF-808-SO_4 sample in a 20 mL glass vial inside the glovebox. The suspension was stirred every 30 min, and after 4 h, the color of the solid was then recorded.

Temperature-programmed desorption with methanol (TPD-methanol)

This procedure involves the controlled adsorption of methanol onto the material's surface, followed by a gradual increase in temperature under an inert gas flow. The desorbed products are monitored using mass spectrometry or gas chromatography. This technique allows for the evaluation of Brønsted acidity, indicated by the formation of dimethyl ether (DME), which is detected through its characteristic signal (m/z = 45). Additionally, the temperature where the DME desorption occurs provides insight into the strength of the acid sites (weak or strong).

Titration with *n*-butylamine in acetonitrile

This technique allows the determination of both the acid strength and the density of acidic sites present in the material.[26] The procedure involves the gradual addition of *n*-butylamine in acetonitrile to the solid sample, enabling selective interaction with the acidic sites. The amount of adsorbed amine is correlated with the concentration of accessible acidic sites on the material's surface.[26]

Catalytic tests

The procedure for this test was based on the published literature with some adjustments.[9] Before the catalytic test, MOF-808-SO_4-Zr and MOF-808-SO_4-Hf were activated at 150 °C for 24 hours under vacuum. The acetalization of benzaldehyde was carried out at 25 °C and atmospheric pressure in a septum-sealed glass reactor charged with 10 mL of methanol, 35 mg of naphthalene as an internal standard, 330 μL of benzaldehyde and 13 mg of the catalyst (MOF-808-SO_4-Zr or MOF-808-SO_4-Hf). The conversion of the reaction was monitored by taking aliquots at different time intervals for analysis by gas chromatography (GC) on a Shimadzu GC-2030 equipped with a flame ionization detector (FID). The mixture was stirred at 500 rpm for 180 minutes for all materials. To test the reuse of the catalyst, MOF-808-SO_4-Zr was recovered after catalysis, washed with water (once) and acetone (twice), dried in an inert atmosphere and finally activated at 150 °C for 12 hours.

Computational details

In this work, we present a set of calculations aimed at investigating the interactions between benzaldehyde and methanol with the materials known as MOF-808-SO_4-Zr or MOF-808-SO_4-Hf. Our focus with the theoretical calculations is specifically on examining how methanol and benzaldehyde interact at the acid sites (Brønsted acid sites). Drawing on previous studies cited in the literature, we performed simulations by isolating a finite fragment of the MOFs, employing a cluster model approach.[27,28] This methodology enables the simulation of the material's electronic characteristics using theoretical frameworks and methodologies available in molecular modeling software.[29] Our cluster model is particularly informed by the coordination structure model and the periodic S-MOF-808 data, as reported by Bo Yang *et al.*[30] These authors were inspired by the initial coordination structure model introduced by Yaghi *et al.*[20] This reduced model comprises two chelating sulfate ligands ($-SO_4^{2-}$), two hydroxo ligands (–OH), and six aqua ligands (H_2O) for each node. Therefore, in this study, we used a cluster model composed of $[M_6O_4(OH)_4(BTC)_6(SO_4)_2(OH)_8(H_2O)]$, where M represents either Zr^{4+} or Hf^{4+} atoms; see Fig. S14† for the representation of the cluster model used. The calculations were performed using Density Functional Theory (DFT) as implemented in the Amsterdam Density Functional (ADF2023) software suite.[31] Given the significant influence of relativistic effects on the chemical and physical properties of heavy elements and their compounds,[24] the zeroth-order regular approximation (ZORA) method was applied to account for these effects.[32] Geometry optimizations were initially carried out using the generalized gradient approximation (GGA) with the Becke–Perdew (BP86) exchange-correlation functional,[33] employing the standard Slater-type orbital (STO) basis set enhanced with two polarization functions (STO-TZ2P).[34] In the first step, the acidity of these materials was analyzed through proton affinity (PA) calculations, as proposed by Bo Yang *et al.*[30] The systems were constructed based on the deprotonation of protons from the aqua ligands and protons from μ_3-OH hydroxo groups. The PA was computed, as indicated in eqn(1):

$$PA = E(MOF^-) + E(H^+) - E(MOF\text{-}H) \quad (1)$$

Here, $E(MOF^-)$ refers to the system considering deprotonation from an aqua ligand or μ_3-OH hydroxo groups. The second term $E(H^+)$ refers to the proton that results from the previous deprotonation. The third term E(MOF-H) accounts for the system without deprotonation.

In the second step, the interactions between the host and guest were examined using energy decomposition analysis (EDA) as outlined by the Morokuma–Ziegler scheme.[35,36] This analysis was carried out using the Amsterdam Density Functional (ADF) package.[31] The systems were separated into two components: MOF-808-SO_4-M, referred to as the host, and the guest, which could be either benzaldehyde or methanol. The interaction energy (ΔE_{Int}) between the two fragments is divided into four components, as demonstrated in eqn (2):

$$\Delta E_{Int} = \Delta E_{Pauli} + \Delta E_{Elec} + \Delta E_{Orb} + \Delta E_{Disp} \quad (2)$$

Here, ΔE_{Pauli} represents the Pauli repulsion, which arises from the interaction between the occupied orbitals of the two molecular fragments. The second term, ΔE_{Elec}, refers to the classi-

cal electrostatic interaction between the two fragments. The third term, ΔE_{Orb}, accounts for possible interactions involving molecular orbitals (MOs), including effects such as charge transfer, polarization, and related processes. Finally, ΔE_{Disp} represents the dispersion forces between the fragments and has been incorporated using Grimme's D3 dispersion correction in the EDA calculations.[37] For all systems, the interaction energies between the host and guest were corrected using the counterpoise method to compensate for the basis set superposition error (BSSE).[38]

Results and discussion

MOF characterization

MOF-808-SO_4-Zr and MOF-808-SO_4-Hf were synthesized following a previously reported method.[19] The materials were subsequently analyzed using various characterization techniques, as shown in Fig. 1.

To assess the structure and crystallinity of the MOFs, PXRD measurements were performed. The diffraction patterns obtained experimentally were compared with those from Rietveld refinement (Fig. 1A), confirming the successful formation of MOF-808-SO_4. The similarity of the diffraction patterns further corroborates the isoreticular nature of MOF-808-SO_4-Zr and MOF-808-SO_4-Hf with their respective precursors, MOF-808-Zr and MOF-808-Hf (see ESI, Fig. S3†).[24]

The porosity of the materials was analyzed through nitrogen adsorption–desorption measurements. To further investigate the functional groups present, FT-IR spectroscopy was performed (Fig. 1B). Both MOF-808-SO_4-Zr and MOF-808-SO_4-Hf exhibit a distinct ν(S═O) stretching vibration at 1049 cm^{-1}, a signal absent in their precursor materials (MOF-808-Zr and MOF-808-Hf) (see ESI, Fig. S3†).[19,24,39] This supports the successful incorporation of sulfate groups into the MOF structures.

The adsorption isotherms (Fig. 1C) exhibit a Type I profile, characteristic of microporous materials. The specific surface areas of MOF-808-SO_4-Zr and MOF-808-SO_4-Hf are 626 m^2 g^{-1}

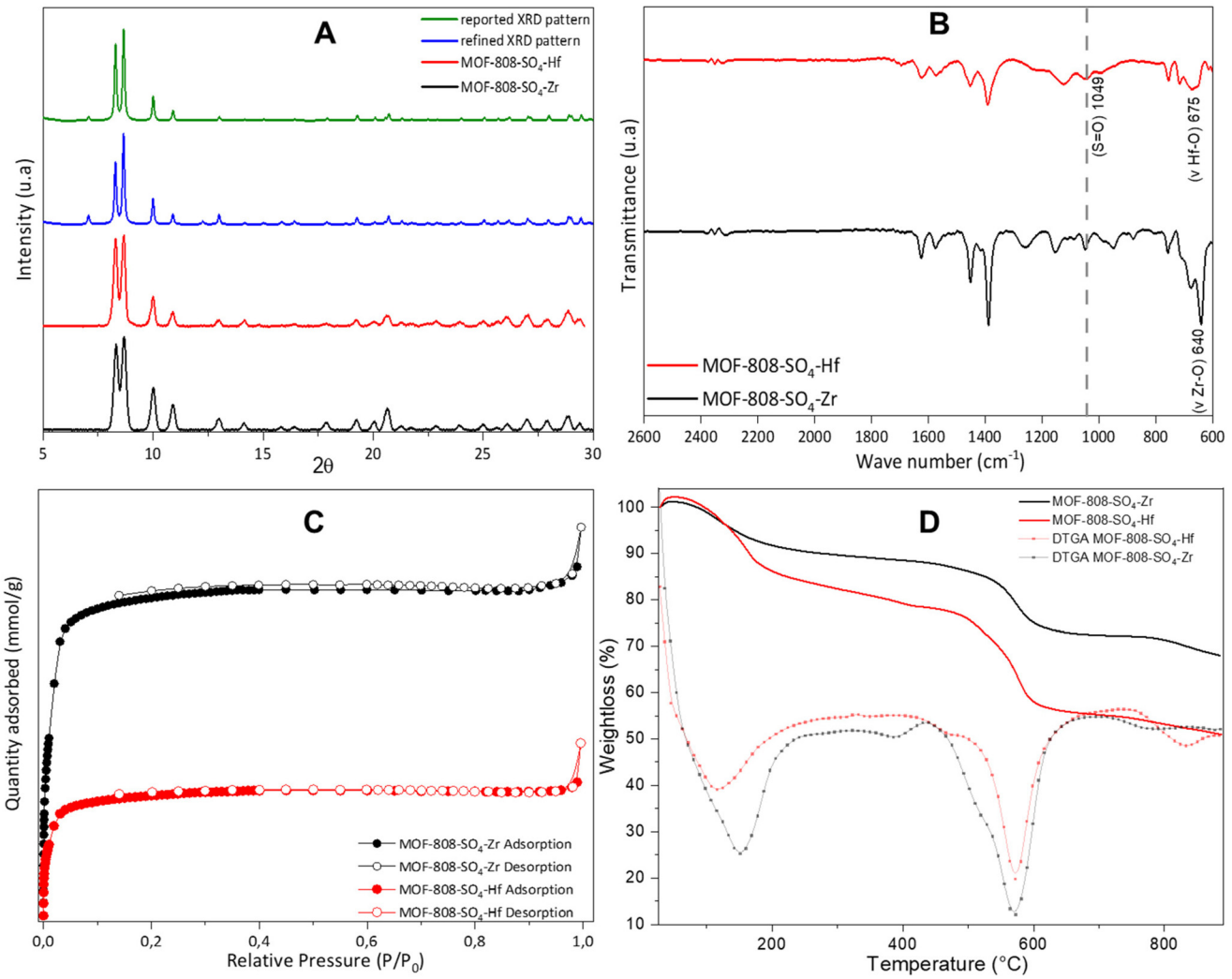

Fig. 1 Characterization of MOF-808-SO_4-Zr and MOF-808-SO_4-Hf: (A) PXRD patterns; (B) ATR-FTIR spectra; (C) nitrogen adsorption–desorption isotherms; and (D) TGA analysis.

and 222 m^2 g^{-1}, respectively. According to the Horvath–Kawazoe (HK) method, the pore size distributions were found to be 5–18 Å for MOF-808-SO_4-Zr and 7–16 Å for MOF-808-SO_4-Hf (see ESI, Fig. S2†). On the other hand, the non-sulfated precursors (MOF-808-Zr and MOF-808-Hf) exhibited BET surface areas of 1339 m^2 g^{-1} and 958 m^2 g^{-1}, respectively. Thus, a significant decrease in surface area is observed after sulfation (see Table S1 in the ESI†). This reduction is attributed to the incorporation of sulfate groups into the framework, whose larger volume relative to formate groups leads to partial pore blockage. These values are notably lower than those of the parent MOF-808 materials MOF-808-Zr (1339 m^2 g^{-1}) and MOF-808-Hf (958 m^2 g^{-1}) due to the presence of sulfate groups, which partially occupy the pores (see ESI, Fig. S4†).[24]

The thermal stability of MOF-808-SO_4-Zr and MOF-808-SO_4-Hf was evaluated using TGA (Fig. 1D). Both materials exhibited three distinct weight loss events, similar to their precursor MOFs.[24] The first weight loss, occurring between 150 and 180 °C, corresponds to the desorption of physisorbed water and residual solvent molecules trapped within the MOF pores.[9] The second weight loss, observed at ~380 °C, is attributed to the release of residual H_2SO_4 molecules that remained within the pores after synthesis. Finally, the third decomposition event, occurring around 580 °C, corresponds to the thermal degradation of the organic linkers, leading to the complete collapse of the MOF structure.[19,21] In comparison, the precursor materials, MOF-808-Zr and MOF-808-Hf, also exhibit three weight loss steps. However, a notable difference is observed in the first two decomposition events, where the precursors show mass losses at 105 °C and 264 °C, which are attributed to the desorption of water molecules and residual synthesis solvents, respectively (see ESI, Fig. S5†).[24] These findings support that the introduction of sulfate groups in MOF-808-SO_4-Zr and MOF-808-SO_4-Hf influences their thermal behavior by altering the nature of the trapped molecules within the framework.

Furthermore, scanning electron microscopy (SEM) was used to examine the morphology of MOF-808-SO_4-Zr (Fig. 2A) and MOF-808-SO_4-Hf (Fig. 2B) after their modification with sulfate groups. In both cases, the materials retained their characteristic octahedral microcrystalline structure (see ESI, Fig. S6†), with particle sizes ranging between 300 and 800 nm. This supports that the post-synthetic modification did not alter the overall morphology of the MOFs.[24] To further validate the elemental composition of the materials, Energy-Dispersive X-ray Spectroscopy (EDS) analyses were performed. The results confirmed the presence of the expected metal centers, with 30% Zr(IV) for MOF-808-SO_4-Zr and 57% Hf(IV) for MOF-808-SO_4-Hf (see ESI, Fig. S7†). Additionally, both materials exhibited a sulfur content of approximately 7%, supporting the successful incorporation of sulfate groups into the structure.

Considering that the structural unit of MOF-808 consists of a Zr_6 (or Hf_6) metal cluster, typically coordinated by six formate groups after synthesis, the number of formates replaced by sulfate anions was estimated. Based on the sulfur atomic percentage obtained by EDS, it is estimated that approximately three formate groups were substituted by sulfate, yielding an average composition of $Zr_6O_4(OH)_4(BTC)_2(SO_4)_3$, which can be abbreviated as MOF-808-3SO_4-Zr.

The superacidity of the prepared materials was evaluated using the Hammett indicator test, a well-established method for determining the acidity of superacidic materials such as zeolites and sulfated zirconia.[40] In this method, the MOFs were immersed in various indicators with known pK_a values, including 4-nitrotoluene (−11.4), anthraquinone (−8.1), 2,4-dinitroaniline (−4.4), 4-nitrodiphenylamine (−2.4), and 2-nitroaniline (−0.2). The color change observed indicated the protonation of each indicator, confirming the acidity of the materials. MOF-808-SO_4-Zr exhibited color changes corresponding to all indicators, transitioning to yellow-red hues, confirming its superacidity in the range of $-0.2 \geq H_0 \geq -11.4$.

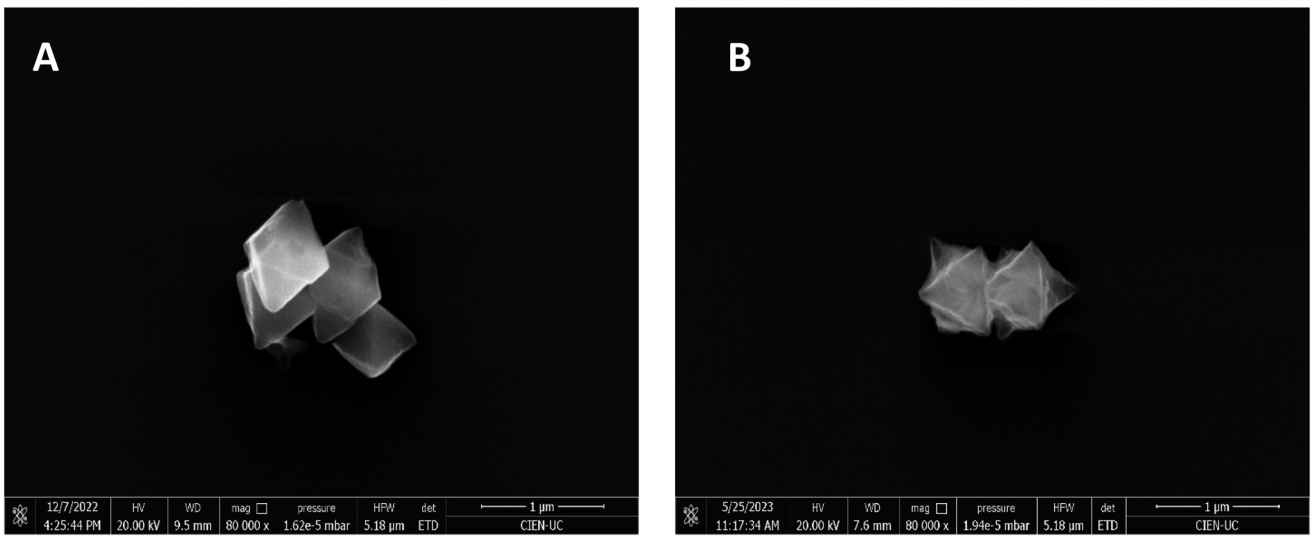

Fig. 2 SEM images of (A) MOF-808-SO_4-Zr and (B) MOF-808-SO_4-Hf.

Meanwhile, MOF-808-SO_4-Hf showed positive results in three indicators, indicating a slightly narrower acidity range of $-4.4 \geq H_0 \geq -11.4$. Compared with its reported analogue MOF VNU-11-SO_4, which exhibits a color change in the presence of 2,4-dinitrofluorobenzene with a value of $H_0 \leq -14.5$, its superacidity is lower than that of the modified material in this research.[41] These results support that both materials exhibit strong acidity, with MOF-808-SO_4-Zr exhibiting slightly higher acidity than its hafnium-based counterpart. The findings further reinforce the effectiveness of sulfate functionalization in enhancing the acidity of these MOFs (see ESI, Table S2†).

In the XPS analysis of MOF-808-SO_4-Zr materials before and after catalysis (see ESI, Fig. S8†), two clearly distinguishable species are observed in the S2p region. The doublet at 168.8/170.5 eV corresponds to sulfate ions (SO_4^{2-}) that are physically adsorbed or weakly interacting with the pores or defects of the MOF. In contrast, the more shifted doublet at ~170.5/171.8 eV suggests a stronger coordination of the sulfate ion to the metal sites of MOF-808, likely forming a functionalized species of the type Zr-OSO_3. This shift indicates a strong electronic interaction, possibly due to a coordinate bond between the oxygen atoms of the sulfate and the Zr centers. The coordination of sulfur to the Zr metal node enhances the Lewis acidity of the cluster, favoring reactions involving the activation of polar bonds, such as C═O or C═C. This coordination is further evidenced by the shift of the S2p peak toward higher binding energies in the XPS spectra. Nattapol Ma *et al.* reported the association of this shift with a decrease in electron density around the sulfur atom as a result of its coordination to the metal.[42]

On the other hand, for MOF-808-SO_4-Hf, no significant coordination of sulfur to the Hf cluster was observed. This represents a key surface difference that may affect the nature of the active sites and, consequently, the catalytic performance of the material (see ESI, Fig. S9†).

Catalytic activities

After characterizing the synthesized materials, their catalytic performance was evaluated in the acetalization reaction of benzaldehyde with methanol. As shown in Fig. 3A, MOF-808-SO_4-Zr exhibited a benzaldehyde conversion exceeding 90% after 60 minutes of reaction, demonstrating its high catalytic activity. In contrast, MOF-808-SO_4-Hf showed a significantly lower conversion, not exceeding 14% within the same reaction time. It is important to note that both sulfated MOFs outperformed their precursors, MOF-808-Zr and MOF-808-Hf, which exhibited minimal catalytic activity, with conversions below 3%.[24] This highlights the role of sulfate functionalization in enhancing the acidity and catalytic efficiency of the materials. The disparity in catalytic performance between MOF-808-SO_4-Zr and MOF-808-SO_4-Hf can be primarily attributed to the significant difference in their surface areas, which directly influences the accessibility of active sites. Despite Hf and Zr having similar physicochemical properties, the higher oxophilicity of Hf with respect to Zr should imply a stronger Brønsted acidic character of the μ_3-OH groups present on the metal node. However, as shown by DFT calculations, the Mulliken charge of the Zr atom (2.57) shows a more positive value than that of the Hf atom (2.35); thus, in the obtained SBU, Zr shows a higher reactivity than Hf. Further explanation can also be found in the DFT section, *vide infra*. Additionally, to assess the structural stability of MOF-808-SO_4-M, PXRD analysis was performed after the catalytic cycle (see ESI, Fig. S1†). The results revealed a notable loss of crystallinity and structural integrity for MOF-808-SO_4-Hf, suggesting that MOF-808-SO_4-Hf undergoes partial degradation under the reaction conditions, which may further contribute to its lower catalytic performance.

Additionally, *n*-butylamine titration was performed to determine the acid strength of the materials, following a previously reported protocol.[26] As shown by this protocol, a larger poten-

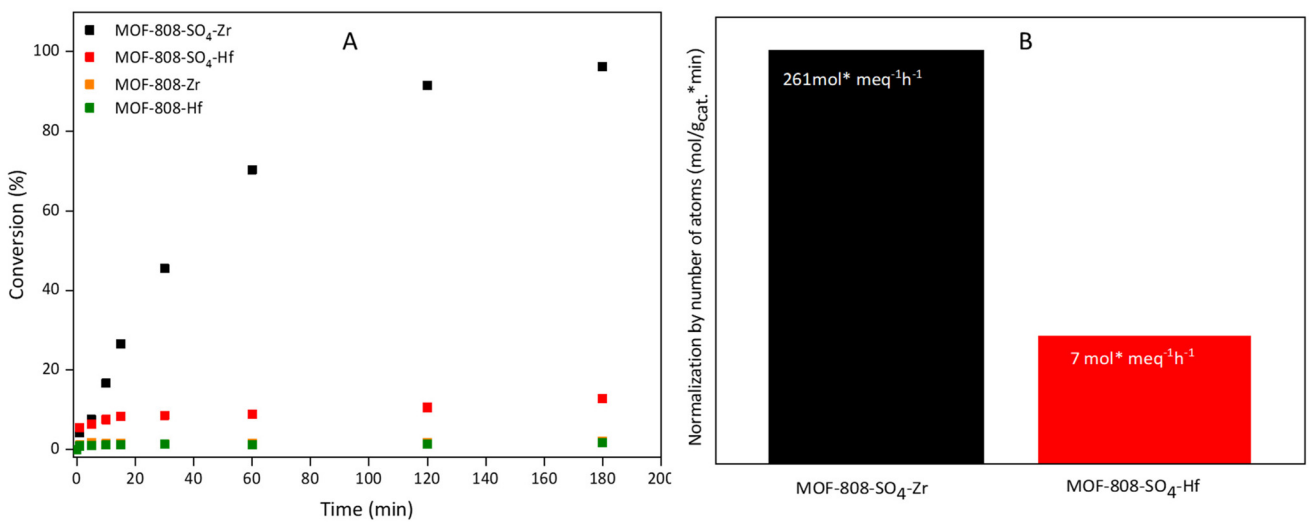

Fig. 3 Conversion *versus* time in the acetalization of benzaldehyde with methanol catalyzed by MOF-808-SO_4-Zr and MOF-808-SO_4-Hf compared to MOF-808-Zr and MOF-808-Hf (A); intrinsic initial rate for MOF-808-SO_4-Zr and MOF-808-SO_4-Hf normalized by the number of metal centers (B).

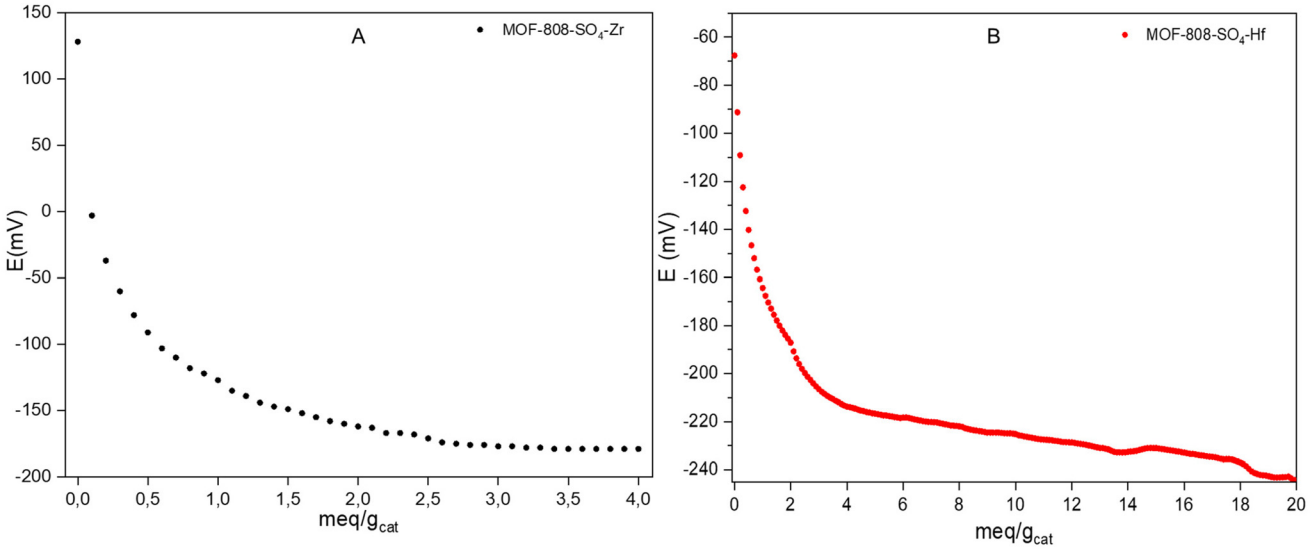

Fig. 4 Potentiometric titration curves with butylamine in acetonitrile for MOF-808-SO_4-Zr (A) and MOF-808-SO_4-Hf (B).

tiometric value for a catalyst correlates with stronger acidity of the catalytic centers. In this sense, the initial electrode potential for MOF-808-SO_4-Zr was measured at 128 mV (Fig. 4A), indicating the presence of very strong acid sites. In contrast, MOF-808-SO_4-Hf exhibited a significantly lower initial electrode potential of −68 mV (Fig. 4B), suggesting the presence of weak acid sites. This difference in acid strength provides an explanation for the variation in catalytic activity observed in the benzaldehyde acetalization reaction. Thus, the higher acidity of MOF-808-SO_4-Zr directly correlates with its superior catalytic performance, while the weaker acid sites in MOF-808-SO_4-Hf contribute to its significantly lower conversion rate. Furthermore, the precursors (MOF-808-Zr and MOF-808-Hf) showed smaller acid strength values, consistent with those reported in previous reports[43] (values of −37 and −28 mV, respectively). These results provide evidence of an increase in acid strength, which could be associated with the incorporation of superacid sites into the sulfated materials.

From the results of *n*-butylamine titration, together with the total number of acid sites and the specific surface area, the acid site density of each material was determined. MOF-808-SO_4-Zr exhibited an acid site density of 6.38×10^{-3} meq m^{-2}, while MOF-808-SO_4-Hf showed a significantly higher density of 9×10^{-2} meq m^{-2}. However, although MOF-808-SO_4-Hf has a higher acid site density, its acid strength is lower as determined by the Hammett method. In comparison, MOF-808-SO_4-Zr, despite having a lower site density, exhibits a wider acidity range.

To further understand the differences in catalytic performance, the initial rate (r_0) of the reaction was calculated. The initial rate was determined from the slope of the initial conversion curve, normalized to the number of metal centers in each material (Fig. 4B). The results showed that MOF-808-SO_4-Zr exhibited an initial rate of 261 mol meq^{-1} h^{-1}, whereas MOF-808-SO_4-Hf exhibited a significantly lower value of 7 mol meq^{-1} h^{-1}.

These findings support that MOF-808-SO_4-Zr has a greater number of accessible and active acid sites, which correlates with its superior catalytic performance. Although MOF-808-SO_4-Hf has a higher acid site density, its lower initial rate suggests that its acid sites may be less accessible or less effective in catalyzing the reaction.

To further analyze the presence and strength of acid sites, temperature-programmed desorption with methanol (TPD-MeOH) was performed, as shown in Fig. 5. The data obtained were normalized based on the amount of catalyst analyzed. The results revealed that MOF-808-SO_4-Zr exhibited an intense desorption peak at 228 °C, indicating the presence of strong acid sites in its structure. This finding aligns well with the Hammett test results,[44] and the previous titration procedures, further confirming the high acidity of this material. In contrast, MOF-808-SO_4-Hf exhibited only a weak signal at 222 °C, suggesting a lower number of acid sites with significantly weaker acidity. This observation supports the previously discussed differences in catalytic conversion between the two materials. Additionally, in both cases, a signal observed above 550 °C corresponds to the decomposition products of the materials.

Given the high catalytic performance observed for MOF-808-SO_4-Zr, this material was selected to evaluate its stability over multiple catalytic cycles. As shown in Fig. 6, MOF-808-SO_4-Zr maintained a conversion rate above 80% even after four successive reaction cycles, demonstrating its robust catalytic activity. However, due to the limited amount of catalyst recovered after the fourth cycle, no further reactions were performed. To assess any structural changes, the recovered material was analyzed by PXRD. While the characteristic diffraction peaks of the MOF were still present, they appeared broader and less intense, indicating a loss of crystallinity upon repeated use (see ESI, Fig. S1A†). This loss of crystallinity would explain the loss of activity observed for MOF-808-SO_4-Zr catalytic cycles.

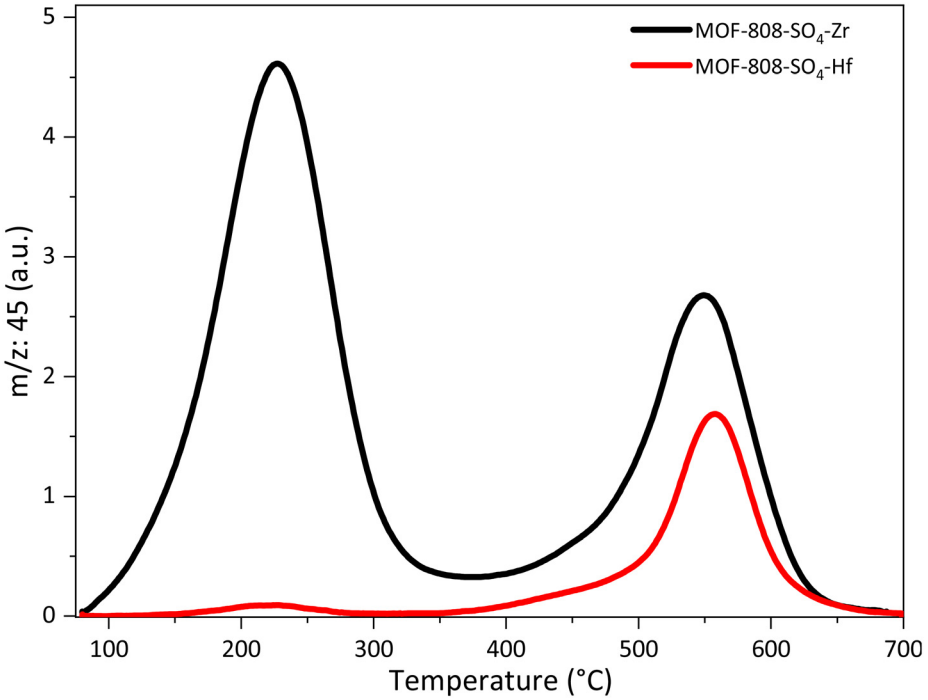

Fig. 5 Temperature-programmed desorption with methanol (TPD-MeOH) for MOF-808-SO_4-Zr and MOF-808-SO_4-Hf.

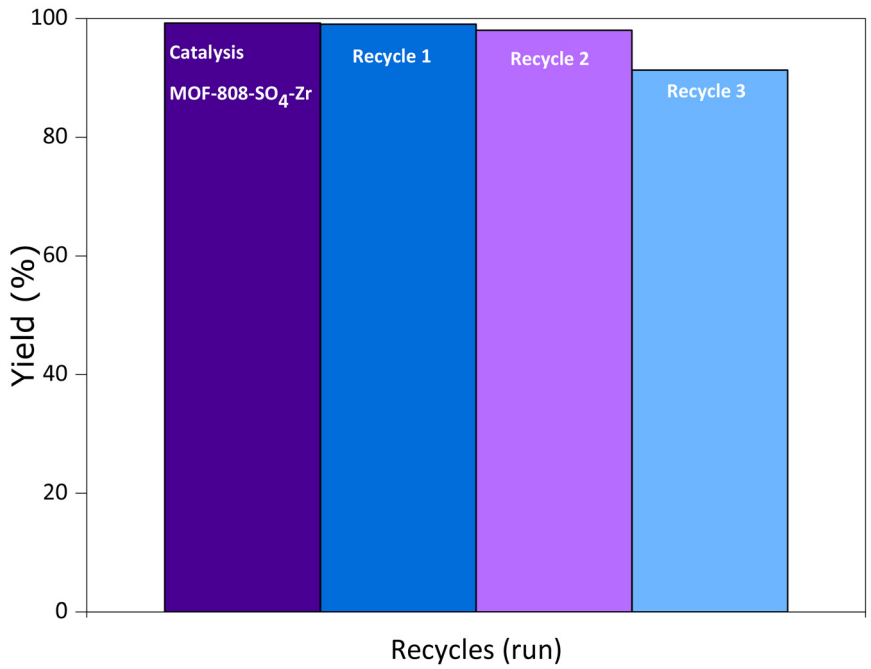

Fig. 6 Recyclability of MOF-808-SO_4-Zr-catalyzed acetalization of benzaldehyde.

Additionally, FT-IR analysis was performed on the recovered MOF-808-SO_4-Zr material after the catalytic cycles (brown color) (see ESI, Fig. S10†). The presence of the band associated with the S=O stretching vibration in the recovered material indicates the retention of the sulfate groups, suggesting the preservation of the structure after the catalytic tests. Furthermore, as mentioned before, the MOF-808-SO4-Zr material exhibits both S2p and Zr3d characteristic signals in post-catalytic test XPS analysis (see ESI, Fig. S8B†). Additionally, scanning electron microscopy (SEM) was performed on the recovered MOF-808-

SO_4-Zr after the catalytic cycles (see ESI, Fig. S11†). A partial loss of the original crystal morphology was observed, along with the formation of aggregates, suggesting partial structural decomposition. Nevertheless, the crystallites retained an average size above 300 nm.

Computational analysis

To evaluate the proton affinities (PAs) in both systems, MOF-808-SO_4-Zr and MOF-808-SO_4-Hf, three types of hydrogen atoms were analyzed. In the case of MOF-Hf, one proton from the μ-hydroxo groups and two protons from aqua ligands were examined, labeled as H1, H2, and H3, as depicted in Fig. S14.† Among the aqua ligands, H2 refers to a proton that interacts with the sulfate ligands, whereas H3 corresponds to a proton from an aqua ligand that does not interact with sulfate ligands. The energy of the PA calculations reveals that the aqua protons H3 and H2 in the MOF-808-SO_4-Zr framework have values of 323 and 330 kcal mol^{-1}, respectively. These results are consistent with previous studies, which reported that the PA values for the twelve aqua protons range from 299 to 336 kcal mol^{-1}. These prior findings were obtained using a cluster model of MOF-808-SO_4-Zr at the M06-L/def2-TZVP theoretical level. For MOF-808-SO_4-Hf, the PA is slightly higher for the aqua protons H3 and H2 compared to MOF-808-SO_4-Zr. For this system, the calculations indicate that the proton affinities of the aqua protons H3 and H2 are 330 kcal mol^{-1} and 340 kcal mol^{-1}, respectively. However, for the protons of the μ-hydroxo groups (H1), this trend is more pronounced, with PA values of 325 kcal mol^{-1} and 305 kcal mol^{-1} for MOF-808-SO_4-Hf and MOF-808-SO_4-Zr, respectively. While the cluster model analysis offers valuable insights into the acidity trend at each node, the presence of numerous Brønsted acid sites in the extended structure of the material limits its scope to a qualitative conclusion; thus, these results should be analyzed together with the previously shown experimental results. All the theoretical results suggest a progressively higher acidity for MOF-808-SO_4-Zr compared to MOF-808-SO_4-Hf. This hypothesis aligns well with our experimental evidence, which confirms the greater acid strength of MOF-808-SO_4-Zr relative to its Hf-based counterpart.

To gain a deeper understanding of the interaction of MOF-808-SO_4-M (host) with both benzaldehyde and methanol (guests), the host–guest interacting systems were considered. An interaction model was used as the starting structure to simulate the MOF-808-SO_4-M/guest interactions for each system. The final conformations of the ground state of the interacting systems indicate intermolecular hydrogen bond (HB) formation, between the protons of μ_3-OH and the benzaldehyde carbonyl group (C═O), for both materials; see Fig. S16(a) and (b).† The calculated lengths of the HBs (μ_3-O–H···O═C–) are 1.818 Å and 1.780 Å, and the angles of μ_3-O–H···O are 168.6° and 164.9° for MOF-808-SO_4-Zr and MOF-808-SO_4-Hf, respectively. In the case of MOF-808-SO_4-M/methanol, in both systems the final conformations show methanol shifted closer to the sulfate ligands, generating a HB (–S–O···H–O–). The calculated lengths of the hydrogen bonds H···O are 1.932 Å and 2.062 Å, and the –O–H···O angles are 156.5° and 173.4° for MOF-808-SO_4-Zr and MOF-808-SO_4-Hf, Fig. S9(c) and S9(d),† respectively. It is noteworthy that these hydrogen bonds satisfy the criteria for intermolecular hydrogen bonding, as their O···H distances are less than 2.45 Å.[45,46]

Based on these results, to get more insights into these interactions in the ground state, an analysis using the EDA scheme was performed. In the fragmentation scheme the MOF-808-SO_4-M and benzaldehyde, were employed as fragments. As shown in Table 1, the host–guest interaction energies suggest that the interactions between MOF-808-SO_4-M and benzaldehyde have very similar values, which do not support the large difference observed in the catalytic activity. However, the decomposition analysis of the interaction energies reveals important differences.

The EDA analysis results show that the electrostatic component (ΔE_{Elect}) is the most important stabilizing term in the two systems, which represented 41% and 38% of the total stabilizing energy, for MOF-808-SO_4-Zr/benzaldehyde and MOF-808-SO_4-Hf/benzaldehyde, respectively. However, the dispersive forces (van der Waals) that act between the MOF-808-SO_4-M and benzaldehyde are also significant; specifically the dispersion component (ΔE_{Disp}) represented 35% of the total stabilizing energy in the case of MOF-808-SO_4-Zr and 36% for the MOF-808-SO_4-Hf material. Finally, in both systems, the contribution of the total orbital interaction (ΔE_{Orb}) accounts for 25% of the overall interaction energy.

From the simulation of the host–guest interaction, we hypothesize that the significant number of Brønsted acid sites and their respective PA values contribute to the difference in acid strength between the materials. In particular, the hydrogen bonding arising from the donor–acceptor interaction between the μ_3-OH protons of these materials and the carbonyl group of benzaldehyde may play a critical role in the catalytic conversion during the benzaldehyde acetalization reaction.

Table 1 Morokuma–Ziegler scheme energy decomposition analysis (EDA), values in kcal mol^{-1}, for the MOF-808-SO_4-M/benzaldehyde and MOF-808-SO_4-M/methanol interacting systems

System	ΔE_{Pauli}	ΔE_{Elect}	ΔE_{Orb}	ΔE_{Disp}	ΔE_{Int}
MOF-808-SO_4-Hf/benzaldehyde	31.07	−21.03(38%)	−13.3(25%)	−19.8(36%)	−23.16
MOF-808-SO_4-Hf/methanol	10.62	−7.21(38%)	−4.97(27%)	−6.56(35%)	−8.13
MOF-808-SO_4-Zr/benzaldehyde	19.58	−15.98(41%)	−9.73(25%)	−13.75(35%)	−19.86
MOF-808-SO_4-Zr/methanol	14.37	−10.54(44%)	−6.08(26%)	−7.19(30%)	−9.44

Conclusion

The post-synthetic modification of MOF-808 was carried out to obtain MOF-808-SO_4-Zr and MOF-808-SO_4-Hf, both of which were thoroughly characterized using structural and textural techniques. Superacidity was determined through the Hammett indicator test, revealing an acidity range of $-0.2 \geq H_0 \geq -11.4$ for MOF-808-SO_4-Zr and $-4.4 \geq H_0 \geq -11.4$ for MOF-808-SO_4-Hf. As heterogeneous catalysts, these materials were tested in the acetalization reaction of benzaldehyde with methanol, where MOF-808-SO_4-Zr demonstrated significantly higher conversion than its Hf-based analogue. *n*-Butylamine titration confirmed the greater acid strength of MOF-808-SO_4-Zr, which was further supported by TPD-MeOH analysis, indicating a higher density of acid sites. Given its superior catalytic performance, MOF-808-SO_4-Zr was reused in four successive cycles, maintaining conversion above 85% in all reactions. Conversely, PXRD analysis of the MOF-808-SO_4-Hf post-reaction revealed a loss of crystallinity, suggesting lower structural stability. Additionally, DFT calculations, incorporating proton affinity (PA) analysis and the energy decomposition analysis (EDA) scheme, were used to explore the MOF-808-SO_4-M interactions with benzaldehyde and methanol. Computational and experimental results confirm that Zr-based frameworks exhibit higher acidity than their Hf-based counterparts, which is attributed to the Brønsted acid sites and their stronger interactions with substrates, ultimately enhancing catalytic efficiency in benzaldehyde acetalization.

Data availability

The data supporting this article have been included as part of the ESI.†

Conflicts of interest

There are no conflicts to declare.

Acknowledgements

The authors thank FONDECYT projects 1231194, 1241917, and ANID Postdoctoral 3230141, as well as ANID/FONDAP/1523A0006. This material is based upon work supported by the Air Force Office of Scientific Research under award number FA8655-25-1-8759. The authors also thank ANID Concurso equipamiento científico y tecnológico FONDEQUIP mediano 2022 codigo EQM 220028 "Adquisición de un Microscopio Electrónico FE-SEM para el fortalecimiento de la investigación, vinculación y docencia de pre y postgrado de la Universidad de Antofagasta". Unidad de Equipamiento Científico MAINI®-XPS, ANID-FONDEQUIP EQM140044. This investigation received financial support from the European Comission through the H2020-MSCA-RISE-2020 BIOALL project (GrantAgreement: 101008058).

References

1 Y. H. P. Zhang, Reviving the Carbohydrate Economy via Multi-Product Lignocellulose Biorefineries, *J. Ind. Microbiol. Biotechnol.*, 2008, 367–375, DOI: 10.1007/s10295-007-0293-6.
2 S. Yokoyama, K. Jonouchi and K. Imou, Energy Production from Marine Biomass : Fuel Cell Power Generation Driven by Methane Produced from Seaweed, *Eng. Technol.*, 2007, **22**(4), 320–323.
3 A. Hornung, *Transformation of Biomass: Theory to Practice*, 2014, DOI: 10.1002/9781118693643.
4 Y. Zheng, J. Zhao, F. Xu and Y. Li, Pretreatment of Lignocellulosic Biomass for Enhanced Biogas Production, in *Progress in Energy and Combustion Science*, Elsevier Ltd, 2014, pp. 35–53. DOI: 10.1016/j.pecs.2014.01.001.
5 C. Somerville, Cellulose Synthesis in Higher Plants, *Annu. Rev. Cell Dev. Biol.*, 2006, 53–78, DOI: 10.1146/annurev.cellbio.22.022206.160206.
6 B. H. Davison, J. Parks, M. F. Davis and B. S. Donohoe, 3 Plant Cell Walls: Basics of Structure, Chemistry, in *Accessibility and the Influence on Conversion*, 2013, pp. 22–38. DOI: 10.1002/9780470975831.ch3.
7 J. Zakzeski, P. C. A. Bruijnincx, A. L. Jongerius and B. M. Weckhuysen, The Catalytic Valorization of Lignin for the Production of Renewable Chemicals, *Chem. Rev.*, 2010, **110**(6), 3552–3599, DOI: 10.1021/cr900354u.
8 E. Nieddu, M. Cataldo, F. Pinna and G. Strukul, in *Acetalization of Ct,13-Unsaturated Carbonyl Compounds Catalyzed by Complexes of Pt(II)*, 1999, vol. 40.
9 E. Camu, C. Pazo, D. Becerra, Y. Hidalgo-Rosa, D. Paez-Hernandez, X. Zarate, E. Schott and N. Escalona, A New Approach to the Mechanism for the Acetalization of Benzaldehyde over MOF Catalysts, *New J. Chem.*, 2020, **44**(35), 14865–14871, DOI: 10.1039/d0nj02416c.
10 J. L. Dong, L. S. H. Yu and J. W. Xie, A Simple and Versatile Method for the Formation of Acetals/Ketals Using Trace Conventional Acids, *ACS Omega*, 2018, **3**(5), 4974–4985, DOI: 10.1021/acsomega.8b00159.
11 D. J. Cole-Hamilton and R. P. Tooze, in *Homogeneous Catalysis Advantages and Problems*, Springer, 2006, vol. 30, p. 1. DOI: 10.1007/1-4020-4087-3_1.
12 C. D. Wu, Crystal Engineering of Metal-Organic Frameworks for Heterogeneous Catalysis, in *Selective Nanocatalysts and Nanoscience: Concepts for Heterogeneous and Homogeneous Catalysis*, 2011, pp. 271–298. DOI: 10.1002/9783527635689.ch8.
13 M. Lammert, C. Glißmann, H. Reinsch and N. Stock, Synthesis and Characterization of New Ce(IV)-MOFs Exhibiting Various Framework Topologies, *Cryst. Growth Des.*, 2017, **17**(3), 1125–1131, DOI: 10.1021/acs.cgd.6b01512.
14 M. Lammert, M. T. Wharmby, S. Smolders, B. Bueken, A. Lieb, K. A. Lomachenko, D. De Vos and N. Stock, Cerium-Based Metal Organic Frameworks with UiO-66 Architecture: Synthesis, Properties and Redox Catalytic Activity, *Chem. Commun.*, 2015, 12578–12581, DOI: 10.1039/c5cc02606g.

15 Z. Hu, T. Kundu, Y. Wang, Y. Sun, K. Zeng and D. Zhao, Modulated Hydrothermal Synthesis of Highly Stable MOF-808(Hf) for Methane Storage, *ACS Sustainable Chem. Eng.*, 2020, **8**(46), 17042–17053, DOI: **10.1021/acssuschemeng.0c04486**.

16 W. Fan, X. Zhang, Z. Kang, X. Liu and D. Sun, Isoreticular Chemistry within Metal–Organic Frameworks for Gas Storage and Separation, *Coord. Chem. Rev.*, 2021, **443**, 213968, DOI: **10.1016/j.ccr.2021.213968**.

17 B. N. Bhadra and S. H. Jhung, Adsorptive Removal of Wide Range of Pharmaceuticals and Personal Care Products from Water Using Bio-MOF-1 Derived Porous Carbon, *Microporous Mesoporous Mater.*, 2018, **270**, 102–108, DOI: **10.1016/j.micromeso.2018.05.005**.

18 U. S. F. Arrozi, H. W. Wijaya, A. Patah and Y. Permana, Efficient Acetalization of Benzaldehydes Using UiO-66 and UiO-67: Substrates Accessibility or Lewis Acidity of Zirconium, *Appl. Catal., A*, 2015, **506**, 77–84, DOI: **10.1016/j.apcata.2015.08.028**.

19 J. Jiang, F. Gándara, Y. B. Zhang, K. Na, O. M. Yaghi and W. G. Klemperer, Superacidity in Sulfated Metal-Organic Framework-808, *J. Am. Chem. Soc.*, 2014, **136**(37), 12844–12847, DOI: **10.1021/ja507119n**.

20 J. Jiang, F. Gándara, Y. B. Zhang, K. Na, O. M. Yaghi and W. G. Klemperer, Superacidity in Sulfated Metal-Organic Framework-808, *J. Am. Chem. Soc.*, 2014, **136**(37), 12844–12847, DOI: **10.1021/ja507119n**.

21 C. A. Trickett, T. M. Osborn Popp, J. Su, C. Yan, J. Weisberg, A. Huq, P. Urban, J. Jiang, M. J. Kalmutzki, Q. Liu, J. Baek, M. P. Head-Gordon, G. A. Somorjai, J. A. Reimer and O. M. Yaghi, Identification of the Strong Brønsted Acid Site in a Metal–Organic Framework Solid Acid Catalyst, *Nat. Chem.*, 2019, **11**(2), 170–176, DOI: **10.1038/s41557-018-0171-z**.

22 C. Xu, W. Orbell, G. Wang, B. Li, B. K. Y. Ng, T. S. Wu, Y. L. Soo, Z. X. Luan, K. Tang, X. P. Wu, S. C. E. Tsang and P. Zhao, Direct Visualisation of Metal-Defect Cooperative Catalysis in Ru-Doped Defective MOF-808, *J. Mater. Chem. A*, 2024, **12**, 19018–19028, DOI: **10.1039/d4ta01689k**.

23 Z. Hu, T. Kundu, Y. Wang, Y. Sun, K. Zeng and D. Zhao, Modulated Hydrothermal Synthesis of Highly Stable MOF-808(Hf) for Methane Storage, *ACS Sustainable Chem. Eng.*, 2020, **8**(46), 17042–17053, DOI: **10.1021/acssuschemeng.0c04486**.

24 Y. Arellano, C. Pazo-Carballo, V. Roa, Y. Hidalgo-Rosa, X. Zárate, J. Llanos, N. Escalona and E. Schott, Catalytic Evaluation of MOF-808 with Metallic Centers of Zr(IV), Hf (IV) and Ce(IV) in the Acetalization of Benzaldehyde with Methanol, *Dalton Trans.*, 2024, **53**, 16397–16406, DOI: **10.1039/D4DT01959H**.

25 M. Thommes, K. Kaneko, A. V. Neimark, J. P. Olivier, F. Rodriguez-Reinoso, J. Rouquerol and K. S. W. Sing, Physisorption of Gases, with Special Reference to the Evaluation of Surface Area and Pore Size Distribution (IUPAC Technical Report), *Pure Appl. Chem.*, 2015, **87**(9–10), 1051–1069, DOI: **10.1515/pac-2014-1117**.

26 R. Cid and G. Pecchi, Potentiometric Method for Determining the Number and Relative Strength of Acid Sites in Colored Catalysts, *Appl. Catal.*, 1985, **14**(C), 15–21, DOI: **10.1016/S0166-9834(00)84340-7**.

27 T. H. T. Le, D. Ferro-Costas, A. Fernández-Ramos and M. A. Ortuño, Combined DFT and Kinetic Monte Carlo Study of UiO-66 Catalysts for γ-Valerolactone Production, *J. Phys. Chem. C*, 2024, **128**(3), 1049–1057, DOI: **10.1021/acs.jpcc.3c06053**.

28 E. García-Rojas, J. Tapiador, P. Leo, C. Palomino, C. Martos and G. Orcajo, Catalytical Advantages of Hf-MOFs in Benzaldehyde Acetalization, *Catal. Today*, 2024, **434**, 114705, DOI: **10.1016/j.cattod.2024.114705**.

29 J. L. Mancuso, A. M. Mroz, K. N. Le and C. H. Hendon, Electronic Structure Modeling of Metal-Organic Frameworks, *Chem. Rev.*, 2020, 8641–8715, DOI: **10.1021/acs.chemrev.0c00148**.

30 B. Yang, J. I. Wheeler, B. Sorensen, R. Steagall, T. Nielson, J. Yao, J. Mendez-Arroyo and D. H. Ess, Computational Determination of Coordination Structure Impact on Adsorption and Acidity of Pristine and Sulfated MOF-808, *Mater. Adv.*, 2021, **2**(13), 4246–4254, DOI: **10.1039/d1ma00330e**.

31 P. H. T. Philipsen and E. J. Baerends, Cohesive energy of 3*d* transition metals: Density functional theory atomic and bulk calculations, *Phys. Rev. B*, 1996, **54**, 5326, DOI: **10.1103/PhysRevB.54.5326**.

32 E. Van Lenthe, E. J. Baerends and J. G. Snijders, Relativistic Regular Two-Component Hamiltonians, *J. Chem. Phys.*, 1993, **99**(6), 4597–4610, DOI: **10.1063/1.466059**.

33 J. P. Perdew and W. Yue, *Accurate and Simple Density Functional for the Electronic Exchange Energy: Generalized Gradient Approximation*, 1986, vol. 8. DOI: **10.1103/PhysRevB.33.8800**.

34 E. V. Lenthe and E. J. Baerends, *Optimized Slater-Type Basis Sets for the Elements 1–118*; 2003, vol. 24. DOI: **10.1002/jcc.10255**.

35 T. Ziegler and A. Rauk, The Transition State Method, in *On the Calculation of Bonding Energies by the Hartree Fock Slater Method I*, 1977, vol. 46. DOI: **10.1007/BF02401406**.

36 K. Kitaura and K. Morokuma, A New Energy Decomposition Scheme for Molecular Interactions within the Hartree-Fock Approximation, *Int. J. Quantum Chem.*, 1976, **10**(2), 325–340, DOI: **10.1002/qua.560100211**.

37 S. Grimme, J. Antony, S. Ehrlich and H. Krieg, A Consistent and Accurate Ab Initio Parametrization of Density Functional Dispersion Correction (DFT-D) for the 94 Elements H-Pu, *J. Chem. Phys.*, 2010, **132**(15), 154104, DOI: **10.1063/1.3382344**.

38 S. F. Boys and F. Bernardi, The Calculation of Small Molecular Interactions by the Differences of Separate Total Energies. Some Procedures with Reduced Errors, *Mol. Phys.*, 1970, **19**(4), 553–566, DOI: **10.1080/00268977000101561**.

39 W. Mu, S. Du, X. Li, Q. Yu, R. Hu, H. Wei, Y. Yang and S. Peng, Efficient and Irreversible Capture of Strontium Ions from Aqueous Solution Using Metal-Organic

Frameworks with Ion Trapping Groups, *Dalton Trans.*, 2019, **48**(10), 3284–3290, DOI: 10.1039/c9dt00434c.

40 S. J. Lyle, R. W. Flaig, K. E. Cordova and O. M. Yaghi, Facilitating Laboratory Research Experience Using Reticular Chemistry, *J. Chem. Educ.*, 2018, **95**(9), 1512–1519, DOI: 10.1021/acs.jchemed.8b00265.

41 L. H. T. Nguyen, H. T. Vo, H. B. Phan, M. H. Dinh Dang, T. Le Hoang Doan and P. H. Tran, Synthesis of 5-Hydroxymethylfurfural from Monosaccharides Catalyzed by Superacid VNU-11-SO4in 1-Ethyl-3-Methylimidazolium Chloride Ionic Liquid, *RSC Adv.*, 2020, **10**(65), 39687–39692, DOI: 10.1039/d0ra08261a.

42 N. Ma, S. Kosasang, J. Theissen, N. Gys, T. Hauffman, K. I. Otake, S. Horike and R. Ameloot, Systematic Design and Functionalisation of Amorphous Zirconium Metal-Organic Frameworks, *Chem. Sci.*, 2024, **15**, 17562–17570, DOI: 10.1039/d4sc05053c.

43 Y. Arellano, C. Pazo, V. Roa, Y. Hidalgo-Rosa, X. Zarate, J. Llanos, N. Escalona and E. Schott, Catalytic Evaluation of MOF-808 with Metallic Centers of Zr(IV), Hf(IV) and Ce(IV) in the Acetalization of Benzaldehyde with Methanol, *Dalton Trans.*, 2024, **53**(39), 16397–16406, DOI: 10.1039/D4DT01959H.

44 P. A. Clayborne, T. C. Nelson and T. C. DeVore, Temperature Programmed Desorption-FTIR Investigation of C1-C5 Primary Alcohols Adsorbed on γ-Alumina, *Appl. Catal., A*, 2004, **257**(2), 225–233, DOI: 10.1016/j.apcata.2003.07.013.

45 Y. I. Naberukhin and V. P. Voloshin, Distributions of Hydrogen Bond Lifetimes in Instantaneous and Inherent Structures of Water, *Z. Physiol. Chem.*, 2009, **223**, 1119–1131, DOI: 10.1524/zpch.2009.6062.

46 A. Chandra, Dynamical Behavior of Anion–Water and Water–Water Hydrogen Bonds in Aqueous Electrolyte Solutions: A Molecular Dynamics Study, *J. Phys. Chem. B*, 2003, **107**(16), 3899–3906, DOI: 10.1021/jp022147d.